

MUSE: The MUon Scattering Experiment

E. Cline¹, J. Bernauer^{1,2}, E.J. Downie³ and R. Gilman^{4*}

¹ Stony Brook University, Stony Brook, NY

² Riken BNL Research Center, Upton, NY

³ The George Washington University, Washington, DC USA

⁴ Rutgers, The State University of New Jersey, Piscataway, NJ

* rgilman@physics.rutgers.edu

February 24, 2021

PAUL SCHERRER INSTITUT



Review of Particle Physics at PSI

doi:[10.21468/SciPostPhysProc.2](https://doi.org/10.21468/SciPostPhysProc.2)

Abstract

MUSE is a high-precision muon scattering experiment aiming to determine the proton radius. Muon, electron, and pion scattering will be measured at the same time. Two-photon exchange corrections will be determined with data using both beam polarities.

23.1 Introduction

The charge radius is a fundamental property of the proton. It is of interest to hadronic physicists as a test of calculations of proton structure. It is of interest to atomic physicists as it affects the determination of the Rydberg constant, and so is important in precision tests of quantum electrodynamics.

The charge radius can be determined using electromagnetic interactions in two ways. In atomic physics, the proton size changes the energies of S states by

$$\Delta E = \langle \Psi_S | \delta V | \Psi_S \rangle = \frac{2}{3} \pi \alpha |\Psi_S(0)|^2 r_p^2, \quad (23.1)$$

thus allowing the radius and Rydberg constant to be determined simultaneously by measuring pairs of transition energies. In electron-proton scattering, the differential cross section depends on the square of the form factor, which is the momentum-space charge distribution. The charge radius is extracted from the slope of the electric form factor G_E at $Q^2 = 0$:

$$r_p^2 = -6 \frac{dG_E}{dQ^2} \Big|_{Q^2=0}. \quad (23.2)$$

As the scattering data do not extend to $Q^2 = 0$, the radius is extracted from fits to measured cross sections.

In 2010 the proton charge radius was determined to be 0.84184 ± 0.00067 fm from a measurement of muonic hydrogen by the PSI CREMA collaboration [1]. This was quite puzzling as it was about 5σ smaller than the nearly order-of-magnitude less precise electronic measurements [2], which used both hydrogen spectroscopy and electron-proton scattering. This proton radius puzzle was quickly confirmed with reports from two new electron scattering measurements yielding $r_p = 0.879 \pm 0.008$ fm [3] and 0.875 ± 0.010 fm [4], and a second measurement of muonic hydrogen [5] that found $r_p = 0.84087 \pm 0.00039$ fm. New data are needed to resolve the proton radius puzzle, and a number of new experiments were developed [6–9]. Most aim to improve existing results, with new measurements of atomic hydrogen or electron-proton scattering. A new set of muonic atom measurements were also undertaken with other light nuclei.

38 23.2 The MUSE experiment

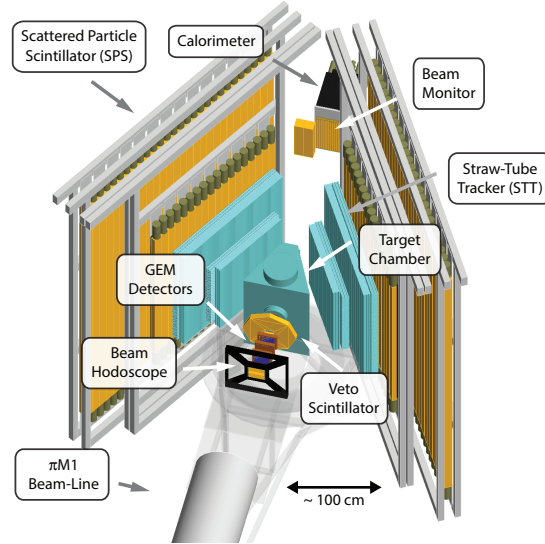


Figure 23.1: The MUSE experimental system. See text for details.

39 The MUon Scattering Experiment (MUSE) addresses the radius puzzle in a unique way. The
 40 intent is to extract the first precise proton radius measurement from muon-proton scattering.
 41 The experiment uses the PSI HIPA PiM1 channel [10, 11], which provides a secondary beam of
 42 pions, muons, and electrons. This enables simultaneous measurements of both electron and
 43 muon scattering, so that the extracted proton radii and the cross sections for the two reactions
 44 can be directly compared. The PiM1 channel can produce beams with similar beam properties
 45 for both polarities. A difference between the scattering probability for the two beam polarities
 46 would result from two-photon exchange, a higher-order correction to the interaction. This
 47 correction is expected to be small, $O(0.1 - 1\%)$, depending on kinematics, but it is difficult to
 48 calculate accurately. It might affect the determination of the radius.

49 Figure 23.1 shows the experimental apparatus, taken from the MUSE Geant4 simulation.
 50 Beam particles exiting the channel first pass through a beam hodoscope, which measures par-
 51 ticle times. In conjunction with the accelerator RF signal, these times can be used to de-
 52 termine particle species. The beam next passes through GEM chambers, which measure the
 53 beam-particle trajectories. A veto scintillator is used to suppress background events such as
 54 upstream beam particle decays in flight or scattering from the detectors, leading to particles
 55 passing through the vacuum chamber wall. The target system inside the vacuum chamber
 56 includes a liquid hydrogen cell, an empty cell, solid targets, and a beam focus monitor. The
 57 unscattered beam exits through a thin window, and reaches the downstream beam monitor and
 58 a calorimeter, which are used to study radiative corrections. Scattered particles exit through
 59 thin side windows, are tracked by the straw tube tracker, and their times measured with the
 60 scattered particle scintillators.

61 The PiM1 channel has been used previously for precise pion scattering measurements. This
 62 is feasible as pions are often the dominant species in the beam, and hadronic scattering cross
 63 sections can be orders-of-magnitude larger than electromagnetic cross sections. A primary
 64 challenge of MUSE is to measure precise cross sections for the smaller muonic component of

65 the beam. The first aspect of the challenge is that previous determinations of beam properties
 66 concentrated on the pionic component of the beam, so the properties of the muonic and elec-
 67 tronic components are not as well known. The second aspect is that the experimental system
 68 has to suppress pion scattering while efficiently measuring muon and electron scattering.

69 To address the challenge of beam properties, MUSE has undertaken a program of simula-
 70 tions and measurements. The first step is to simulate the particle production mechanisms at
 71 the M target. Charged pions are produced at the M target through $pC \rightarrow \pi^\pm X$ reactions. From
 72 the perspective of the PiM1 channel, the proton beam crosses the M target generating pions
 73 with an effective millimeter-sized source. Muons are produced by the decays in flight of those
 74 pions. Simulations show that the majority of the muons that will pass through the PiM1 chan-
 75 nel are generated by pions that decay in the first few centimeters of flight, at an angle of nearly
 76 90° in the pion rest frame. The effective muon source size is larger than the pion source size,
 77 but still only a few millimeters. Electrons and positrons are produced mainly by a sequence
 78 of reactions, with $pC \rightarrow \pi^0 X$ producing neutral pions, followed by the decay $\pi^0 \rightarrow \gamma\gamma$, and
 79 subsequently pair production in the M target via $\gamma C \rightarrow e^\pm X$. Geant4 simulations show that
 80 higher momentum electrons and positrons are only produced when all these processes are in
 81 the direction of the PiM1 channel. As a result, the effective source size remains very close to
 82 that for pions.

83 The source simulations generate charged particles that are input to the TURTLE [12] and
 84 G4 beamline [13] magnetic transport codes. These codes include the channel quadrupoles and
 85 dipoles, as well as apertures from beam pipes and jaws. The simulation describes well several
 86 measured properties of the beam, including the beam distributions in position and angle at
 87 the channel intermediate focal plane and at the scattering target position, and the variation of
 88 particle times at the scattering target with respect to accelerator RF as a function of momen-
 89 tum: the pion time distribution is wider than that for electrons or muons due to the interplay
 90 of faster speed vs longer flight path for higher-momentum particles within the channel. While
 91 the measured time distributions of all particles are quite similar, the muon distribution is pre-
 92 dicted to be somewhat larger than the pion and electron distributions, indicating that extreme
 93 rays are more constrained in reality than in the simulation.

94 In addition to the particle trajectories, it is important to know the beam momentum at the
 95 0.2% (0.3%) level for muons (electrons). The channel momentum resolution is better than
 96 this. The absolute momentum of the beam selected by the PiM1 channel is determined in
 97 3 ways. First, dedicated time-of-flight measurements with changes of the beam hodoscope
 98 and beam monitor positions determine the pion and muon momenta to the 0.2 – 0.3% level.
 99 Second, the timing of particles in the beam hodoscope relative to the accelerator RF provides
 100 an independent momentum measurement at the same level.¹ Third, the dispersion of the
 101 channel at the intermediate focal point, of 7 cm/%, combined with the dispersion of the beam
 102 from the intermediate focus to the scattering target of ≈ 9.5 cm/%, provides a check of any
 103 momentum difference between the different particle species at the $\approx 0.1\%$ level, through the
 104 similarity of the measured beam spot positions.

105 The challenge of suppressing pion scattering while efficiently measuring muon and electron
 106 scattering is addressed by the MUSE trigger system. A first-level trigger FPGA identifies all
 107 particle species in the 3.5-MHz beam using the time difference between the beam-hodoscope
 108 signal and the accelerator RF signal. Other first-level triggers identify scattered particles and
 109 hits in the veto detector. The combination of these first-level triggers allows muon and electron
 110 scattering to be read out efficiently while suppressing pion scattering.

111 One important feature of MUSE will be the implementation of a blinded analysis in the
 112 cross section measurement. A Monte Carlo simulation is needed to determine precise cross sec-
 113 tions, and from them the proton radius. The blinding will be accomplished primarily through

¹This timing measurement also checks the beam momentum stability at the $\approx 0.1\% - 0.2\%$ level.

114 modifying the simulation-derived weight factor, while encrypting the actual weights. Addi-
 115 tionally, some small fraction of the tracks for different particle species will be thrown away
 116 as a function of angle, to prevent accidental unblinding by direct comparison of charge and /
 117 or particle species. This will be programmed to be reversed by the application of two encryp-
 118 tion keys. Once the analysis is complete, the actual weights can be extracted and the physics
 119 analysis rerun.

120 A more detailed description of the MUSE system is available in [14]. Detailed publications
 121 are also available for the target [15] and the SiPM detectors [16].

122 23.3 Anticipated results

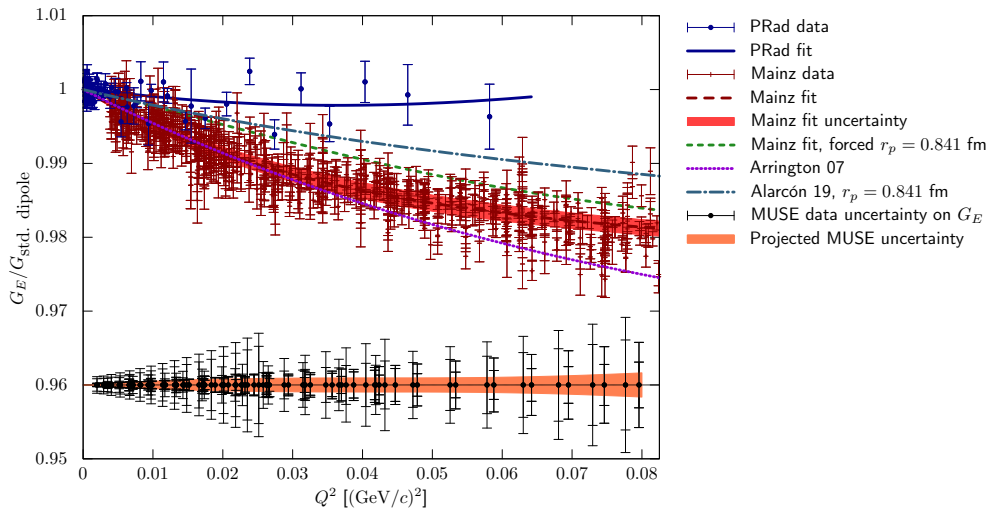


Figure 23.2: Anticipated uncertainty for G_E from MUSE, with its central value arbitrarily placed at 0.96. See text for details.

123 With the planned 12 months of beam time, $4 \times 10^7 \mu^+$ ($2 \times 10^7 \mu^-$) scattering events are
 124 expected for MUSE. This should give better than 1% statistical precision for the cross section
 125 in each of the 16 planned angle bins at each of 3 beam momenta and two beam polarities.
 126 Figure 23.2 shows the expected uncertainties for the determination of the electric form factor,
 127 G_E , from MUSE, together with the results from Mainz [3] and from PRad [17], along with two
 128 selected fits [18, 19]. Both electron and muon results are shown with uncertainties for both +
 129 and - beam polarities. The muon and electron points are slightly offset at higher Q^2 due to their
 130 mass difference. The experiments each measure in different kinematic regions, with MUSE at
 131 the lowest beam momentum and largest angles, and PRad at the highest beam momentum
 132 and smallest angles. The Mainz and PRad data can be seen to diverge from each other, which
 133 probably indicates problems either with the experiments or with the radiative corrections. The
 134 expected MUSE uncertainties are competitive with those of the existing experiments. Muon
 135 scattering has much smaller single-photon radiative corrections, due to its greater mass, so
 136 any differences between muons and electrons might point to issues of radiative corrections or
 137 new physics.

138 The comparison of the cross sections for + and - polarities will yield a measurement of
 139 the two-photon exchange contribution, expected to be of similar size to the experimental un-
 140 certainties shown in Figure 23.2. The proton radius should be determined with an uncertainty
 141 of 0.006 – 0.010 fm, based on a sample of fits. The electron scattering data will have supe-
 142 rior statistical precision, but larger systematic uncertainties due to radiative corrections. This

143 should result in slightly better measurements for both the radius and the two-photon exchange
144 contribution.

145 In addition to the electromagnetic scattering, pion cross sections need to be measured dur-
146 ing MUSE to sufficiently characterize experimental backgrounds. The pion cross sections are
147 interesting by themselves as a test of the application of chiral perturbation theory, to improve
148 the existing πN scattering database, and as a constraint on occasional speculations about
149 undiscovered resonances in the πN system.

150 23.4 Outlook

151 A test of the full MUSE system in December 2019 led to several planned upgrades to make
152 the system more robust. Due to the ongoing international public health crisis and its resulting
153 impact on international travel, we were only able to partially complete the upgrades during
154 2020. We plan to complete the upgrades and start MUSE production data taking in 2021.
155 With 12 months of data taking and analysis to be performed, we anticipate publication of
156 first results in 2023/24. MUSE will be the first experiment to measure elastic muon-proton
157 scattering in an appropriate kinematic region, with a precision sufficient to address the proton
158 radius puzzle. The corresponding results for the simultaneously-measured electron scattering,
159 will put a strong constraint on potential systematic uncertainties, and may help settle the
160 discrepancies between the Mainz and PRad results. MUSE will be the only experiment that
161 can measure the difference between electron and muon extractions of the radius, making it
162 highly compelling.

163 *Acknowledgement:* This work was supported in part by the U.S. National Science Founda-
164 tion, grants PHY-1913653, 2012940 and 2012114.

165 References

- 166 [1] R. Pohl *et al.*, *The size of the proton*, Nature **466**, 213 (2010), doi:[10.1038/nature09250](https://doi.org/10.1038/nature09250).
- 167 [2] P. J. Mohr, B. N. Taylor and D. B. Newell, *CODATA Recommended Values of*
168 *the Fundamental Physical Constants: 2010*, Rev. Mod. Phys. **84**, 1527 (2012),
169 doi:[10.1103/RevModPhys.84.1527](https://doi.org/10.1103/RevModPhys.84.1527), [1203.5425](https://arxiv.org/abs/1203.5425).
- 170 [3] J. Bernauer *et al.*, *High-precision determination of the electric and magnetic form factors of*
171 *the proton*, Phys. Rev. Lett. **105**, 242001 (2010), doi:[10.1103/PhysRevLett.105.242001](https://doi.org/10.1103/PhysRevLett.105.242001),
172 [1007.5076](https://arxiv.org/abs/1007.5076).
- 173 [4] X. Zhan *et al.*, *High-Precision Measurement of the Proton Elastic Form Factor Ratio*
174 $\mu_p G_E/G_M$ *at low Q^2* , Phys. Lett. B **705**, 59 (2011), doi:[10.1016/j.physletb.2011.10.002](https://doi.org/10.1016/j.physletb.2011.10.002),
175 [1102.0318](https://arxiv.org/abs/1102.0318).
- 176 [5] A. Antognini *et al.*, *Proton Structure from the Measurement of $2S-2P$ Transition Frequen-*
177 *cies of Muonic Hydrogen*, Science **339**, 417 (2013), doi:[10.1126/science.1230016](https://doi.org/10.1126/science.1230016).
- 178 [6] R. Pohl, R. Gilman, G. A. Miller and K. Pachucki, *Muonic hydrogen and the proton radius*
179 *puzzle*, Ann. Rev. Nucl. Part. Sci. **63**, 175 (2013), doi:[10.1146/annurev-nucl-102212-](https://doi.org/10.1146/annurev-nucl-102212-170627)
180 [170627](https://arxiv.org/abs/1301.0905), [1301.0905](https://arxiv.org/abs/1301.0905).
- 181 [7] R. Pohl, R. Gilman and G. A. Miller, *Workshop on the proton radius puzzle at the trento*
182 *european center for theory in nuclear physics and related areas* (2012).
- 183 [8] C. Carlson, R. Hill, S. Karshenboim and M. Vanderhaeghen, *Workshop on the proton*
184 *radius puzzle at the mainz institute for theoretical physics* (2014).

- 185 [9] R. Pohl, R. Gilman and G. A. Miller, *Workshop on the proton radius puzzle at the trento*
186 *european center for theory in nuclear physics and related areas* (2016).
- 187 [10] R. Balsiger, B. Berkes, D. Brombach, D. George, M. Ianovici, E. Pedroni, O. Szavits,
188 M. Werner, J. Zichy, E. Boschitz, J.-P. Egger and C. Wiedner, *Technical aspects of the sin*
189 *pion channel and spectrometer*, *Nuclear Instruments and Methods* **157**(2), 247 (1978),
190 doi:[https://doi.org/10.1016/0029-554X\(78\)90298-7](https://doi.org/10.1016/0029-554X(78)90298-7).
- 191 [11] J. P. Albanese, J. Arvieux, E. T. Boschitz, R. Corfu, J. P. Egger, P. Gretillat, C. H. Q. In-
192 gram, C. Lunke, E. Pedroni, C. Perrin, J. Piffaretti, L. Pflug *et al.*, *The SIN high resolu-*
193 *tion pion channel and spectrometer*, *Nuclear Instruments and Methods* **158**, 363 (1979),
194 doi:[10.1016/S0029-554X\(79\)93570-5](https://doi.org/10.1016/S0029-554X(79)93570-5).
- 195 [12] K. L. Brown and C. Iselin, DECAF TURTLE, CERN Report 74-2 (1974).
- 196 [13] T. Roberts, *G4beamline* (2018).
- 197 [14] R. Gilman *et al.*, *Technical Design Report for the Paul Scherrer Institute Experiment R-12-*
198 *01.1: Studying the Proton "Radius" Puzzle with μ p Elastic Scattering* (2017), [1709.09753](https://arxiv.org/abs/1709.09753).
- 199 [15] P. Roy *et al.*, *A Liquid Hydrogen Target for the MUSE Experiment at PSI*, *Nucl. Instrum.*
200 *Meth. A* **949**, 162874 (2020), doi:[10.1016/j.nima.2019.162874](https://doi.org/10.1016/j.nima.2019.162874), [1907.03022](https://arxiv.org/abs/1907.03022).
- 201 [16] T. Rostomyan *et al.*, *Timing detectors with SiPM read-out for the MUSE experiment at*
202 *PSI*, *Nucl. Instrum. Meth. A* **986**, 164801 (2021), doi:[10.1016/j.nima.2020.164801](https://doi.org/10.1016/j.nima.2020.164801),
203 [2007.12207](https://arxiv.org/abs/2007.12207).
- 204 [17] W. Xiong *et al.*, *A small proton charge radius from an electron–proton scattering experiment*,
205 *Nature* **575**(7781), 147 (2019), doi:[10.1038/s41586-019-1721-2](https://doi.org/10.1038/s41586-019-1721-2).
- 206 [18] J. Arrington, W. Melnitchouk and J. Tjon, *Global analysis of proton elastic form fac-*
207 *tor data with two-photon exchange corrections*, *Phys. Rev. C* **76**, 035205 (2007),
208 doi:[10.1103/PhysRevC.76.035205](https://doi.org/10.1103/PhysRevC.76.035205), [0707.1861](https://arxiv.org/abs/0707.1861).
- 209 [19] J. Alarcón, D. Higinbotham, C. Weiss and Z. Ye, *Proton charge radius extraction from*
210 *electron scattering data using dispersively improved chiral effective field theory*, *Phys. Rev.*
211 *C* **99**(4), 044303 (2019), doi:[10.1103/PhysRevC.99.044303](https://doi.org/10.1103/PhysRevC.99.044303), [1809.06373](https://arxiv.org/abs/1809.06373).